

# Design of a novel Electrostatic Ion Storage Ring at KACST

M.O.A. ElGhazaly<sup>1\*</sup>, S.M.Alshammari<sup>1</sup>, C.P.Welsch<sup>2</sup>, H.H.Alharbi<sup>1</sup>

<sup>1</sup>*National Center for Mathematics and Physics (NCMP),*

*King Abdulaziz City for Sciences and Technology (KACST), P.O. Box 6086, Riyadh 11442, Saudi Arabia*

<sup>2</sup>*Cockcroft Institute and the University of Liverpool, UK*

**Abstract.** A new electrostatic storage ring for beams at energies up to 30keV $q$  is currently under development at the National Centre for Mathematics and Physics (NCMP), King Abdulaziz City for Science and Technology (KACST). The ring design is based on the existing electrostatic storage rings, but stretches significantly beyond them in that it shall form the core of a unique flexible experimental facility at KACST. The lattice of this ring has been designed in a way that enables the use of state-of-the-art experimental methods to study electron-ion, laser-ion, and ion-neutral beams interactions. The lattice design also allows for a future upgrade of the ring to a double storage ring structure that would enable ion-ion beam interactions to be performed. In this paper, we present the design of this ring with a focus on beam dynamics calculations for the 7° single-bend racetrack layout. The study is principally based on the SIMION8 program. We complemented this study further by using purpose-written routine and MAD-X simulation code. An in-depth investigation into beam stability under consideration of non-linear field components in the electrostatic optical elements, is presented. Finally, different working points and stability regions are discussed.

**Keywords:** Electrostatic storage devices, Storage rings, SIMION, Fringe fields, Aberrations; Atomic and Molecular physics.

**PACS:** 29.20.Ba , 29.20.D-, 41.75.-i, 41.85.-p

---

## 1. Introduction

Heavy-ion storage rings have provided a great impetus to research in the field of atomic and molecular collisions. In particular, with the advent of a new generation of storage rings relying exclusively on the use of electrostatic optics, applications toward e.g. biological sciences became possible. A distinctive feature of electrostatic storage rings is that there is in principle no limitation to the mass of the ions that can be stored in such rings [1]. This is because the electric field rigidity scales with the kinetic energy-to-charge ratio ( $T/q$ ) of the particle:

-----  
\* Corresponding author. Tel: +966-1-4814401, Fax: +966-1-4814472. E-mail address: maelghazaly@kacst.edu.sa (M O A El Ghazaly).

33 
$$\rho E = \frac{2T}{q} \quad (1)$$

34

35 As the kinetic energy of the particles ( $T$ ) depends only from the acceleration voltage ( $\Delta U_{\text{acc}}$ ) of the high voltage  
36 platform, and the charge state of the particle ( $q$ ), the electrostatic bending is therefore independent of the ion's mass  
37  $m$  and this is in contrast to the magnetic field rigidity, which is mass dependent:

38

39 
$$\rho B = \frac{1}{q} \sqrt{2mT} \quad (2)$$

40

41 Electrostatic rings thus enable the storage of heavy molecular ions and allow for in-depth studies of  
42 macromolecules, such as clusters or large bio-molecular systems, including proteins, amino acids and even DNA  
43 fragments. This opens up new opportunities in interdisciplinary fields such as e.g. biophysics and biochemistry. In  
44 addition to the unique advantage of not being limited in the mass of stored ions, electrostatic rings also benefit from  
45 the absence of hysteresis effects and magnetic remanence, ease of operation, since the number of ion optical  
46 elements is rather small and compact dimensions, keeping overall costs low. Moreover, such rings can be cooled  
47 down to very low temperatures, e.g. by cryo-cooling thereby providing some control of the black-body radiation  
48 induced photo-decay of weakly-bound negative ions [2].

49

50 The first electrostatic storage ring dedicated to research in atomic and molecular physics appeared in 1998. The  
51 Electrostatic Ion Storage ring in Aarhus (ELISA) is a compact racetrack shaped ring of about 7 m circumference  
52 [1]. The concept of ELISA relies on the exclusive use of electrostatic fields to act on the stored ion beam. The  
53 second electrostatic ring was built at the high energy accelerator research organization (KEK) in Tsukuba, Japan [3]  
54 and was an improved version of ELISA, with cylindrical deflectors to bend ions instead of spherical deflectors as  
55 used initially in ELISA. The KEK-ring also features a racetrack lattice of two super periods with mirror symmetry.  
56 Each super period consists of one  $160^\circ$  bending deflector, inserted equidistantly between two  $10^\circ$  Parallel-Plate  
57 Deflectors (PPD), and two quadrupole doublets for beam focusing. Both rings operate at a similar energy range  
58 between 20-25 keV $q$ . Although similar in design, both rings follow a rather different research program, with groups  
59 in Aarhus focusing on measurements of lifetimes of metastable states, cluster dynamics, and photo-excitation of  
60 chromophores of photoactive proteins [4-9]. In terms of interaction with electrons, ELISA relies on the use of an  
61 electron target in a  $90^\circ$  crossed-beam configuration [10], whereas the KEK-ring has a longitudinal electron target

62 used in merged beam geometry, which can also be used to realize some beam cooling [11]. Because of the rather  
63 short interaction length between the electron beam and the stored ion beam, the achievable cooling effect is,  
64 however, somewhat limited. The integrated electron target/cooler is a unique feature of the KEK ring and enabled a  
65 broad research program in electron scattering on bio-molecular ions [12-13]. The electron target at ELISA has been  
66 extensively used with exciting experiments to probe the existence of multiple charge resonance states and their  
67 stabilization upon hydration by single water molecules [14-15]. Comprehensive reviews on the research program at  
68 both rings can be found in [2, 16-18]. A third ring, also relying on a similar racetrack layout has been developed by  
69 the atomic physics and cluster chemistry groups at Tokyo Metropolitan University (TMU) and was constructed by  
70 Toshiba [19]. The TMU E-ring, in short, follows a different vacuum and cooling concept, in which the electrodes  
71 and shields surrounding the nominal trajectory of the stored ions are kept at liquid nitrogen (LN<sub>2</sub>) temperature.  
72 Thereby, the ions cool down mostly to the vibrational ground state [19-20]. Taking advantage of this distinctive  
73 feature, the TMU E-ring has enabled a variety of exciting experiments to be performed, mostly oriented to the  
74 structure and dynamics of clusters, as well as lifetime measurement of multiply charged metastable states [21].

75

76 Based on the success of the broad experimental program that became accessible through the above-mentioned  
77 storage ring facilities, a number of additional electrostatic storage rings have been designed and are presently being  
78 built up or commissioned: An electrostatic storage ring with a design energy of up to 50 keV/q is presently being  
79 commissioned at the Institut für Kernphysik (IKF) at the University of Frankfurt, Germany [22]. The Frankfurt Low  
80 Energy Storage Ring or FLSR in short is optimized to focus the stored beam down to a very small cross section  
81 below 1 mm<sup>2</sup> at the interaction points. In particular, FLSR features a rather large deflection in a PPD with a  
82 deflecting angle of 15°. A ground-breaking concept in terms of both flexibility and cooling has come together with  
83 the development and construction of a double cryogenic storage ring structure; DESIREE (Double ElectroStatic Ion  
84 Ring ExpEriment), at Stockholm University, Sweden [23-24]. The individual storage rings in DESIREE feature a  
85 racetrack layout similar to that of ELISA and derived versions. DESIREE is a unique facility that will enable the  
86 interactions between negative and positive ions to be studied at low and well-defined internal temperatures and  
87 relative energies down to 10 K and 10 meV, respectively. The Cryogenic electrostatic Storage Ring (CSR) that is  
88 being constructed at the Max-Planck Institute for Nuclear Physics in Heidelberg, Germany [25-26] stretches  
89 significantly beyond the preceding rings in e.g. the availability of state-of-the-art techniques and experimental  
90 methods such as a reaction microscope or the use of an ultra-cold electron target, and gas-jet target. CSR features a  
91 quadratic shaped layout with four straight sections interconnected by 90° split-bending corners. In particular, it is

92 designed to operate under extreme vacuum conditions and ultra-low temperatures down to  $\sim 2\text{K}$ , and so it will be a  
93 unique facility in that sense. At the time being, an even miniaturized electrostatic storage ring has been developed  
94 and built at the University of Lyon in France [27]. This tabletop Mini-Ring features a rather different shape and  
95 follows a different optical concept, making use of conical electrostatic mirrors instead of bending deflectors. More  
96 recently, a novel compact cryogenic ion storage ring is now under construction at RIKEN in Japan [28]. This  
97 RIKEN mini cryogenic ring is designed to operate at very low temperatures, down to the temperature of liquid  
98 helium. Another Ultra-low energy electrostatic Storage Ring (USR) will form a central installation in the future  
99 Facility for low-energy Antiproton and Ion Research (FLAIR), at GSI, Germany [29] and a proposal for a new  
100 electrostatic storage ring is currently under discussion at NASA's Jet Propulsion Laboratory [30].

101  
102 At KACST, a highly flexible storage ring for beams at energies up to  $30\text{keV}q$  is presently being developed  
103 to complement this spectrum of facilities. With the right experience gained during the work at the pioneering  
104 Danish storage ring ELISA [14-15], we have been working, here at KACST, on the development of a facility for  
105 atomic and Molecular collisions around an electrostatic storage ring. In this context, a specific design for a highly  
106 flexible storage ring relying on the distinctive features of the existing designs such as of ELISA, FLSR, and  
107 DESIREE [31] has been carried out. Preliminary lattice studies, using MAD-X code, of the basic conceptual design  
108 have been done [32-33]. The conceptual design of such a ring relies on the distinctive features of the existing  
109 designs such as of ELISA, FLSR, and DESIREE [31]. Preliminary lattice studies, using MAD-X code, of this basic  
110 conceptual design have been done [32-33]. Here, we have used the SIMION program to reproduce the exact shape  
111 of electrodes and simulate the fields in the most realistic distribution. Furthermore, changes in the optics  
112 configuration have been imposed by the mechanical design and geometrical constraints, and so lattice calculations  
113 had to be refined. Thereby, the present design study complements preliminary studies and finalizes the design.

114  
115 Although the design concept follows the known preceding electrostatic storage rings, our design has a number  
116 of distinct features that will make this ring a truly unique experimental facility: It has been designed to become the  
117 core of an experimental facility that will allow combining many different, yet complementary beam techniques. The  
118 association of such complementary techniques is projected to enable, for the first time in electrostatic storage ring  
119 experiments, absolute measurement of cross-sections for atomic and molecular collision processes [34].  
120 Furthermore, our design features a rather significantly small deflection in a PPD with a deflecting angle of  $7^\circ$ . The

121 following sections present the details of the design of this 7<sup>o</sup> electrostatic storage ring. The following sections  
122 present the details of this 7<sup>o</sup> design of the KACST electrostatic storage ring.

123 The following sections present the details of the design of this 7<sup>o</sup> electrostatic storage ring  
124

## 125 **2. Linear Ion Beam Optics**

126 All the above storage rings rely on the exclusive use of electrostatic fields for bending and focusing the beam.  
127 These are generated in parallel plate deflectors, cylinder deflectors and electrostatic quadrupoles, and one therefore  
128 refers to *linear beam optics*, i.e. a storage ring where no higher order (sextupole, octupole, etc) fields are used. This  
129 does, however, not mean that there are no higher order multi-pole fields in such storage rings, as fringe fields at the  
130 entrance and exit region of every optical element may have significant higher order components. Their effect on the  
131 stored ion beam needs to be carefully studied as it can dramatically limit beam lifetime and reduce the ring  
132 acceptance and dynamic aperture. In the present study, we addressed the question whether fringe fields compromise  
133 the ability of an electrostatic ring to store beams of low-energy up to 30 keV·q. We first demonstrated that the ring  
134 can efficiently store low-energy beams in spite of existing fringing fields.

135 In order to minimize fringe field effects, grounded shields are normally installed at the entrance and exit of every  
136 deflector. This allows also controlling the geometrical length of the electrodes so that the effective path length  
137 corresponds to the design values [31]. Thereby one can maximize the acceptance and dynamic aperture of the ring.  
138 The only exception to this design concept is the design of the 7<sup>o</sup> parallel-plate deflectors, which are described in  
139 more detail in section 3.1.

140

141 Fringe fields in an electrostatic bend cause a change in the kinetic energy of the particles, which in return get  
142 focused at different image points and one refers to this effect as chromatic aberrations [35]. Spherical aberrations are  
143 rather related to the geometry of the lens and the topology of the lens field. Both, spherical and chromatic,  
144 aberrations can cause limitations in dynamic aperture of an electrostatic ring [36]. Still, in the context of comparing  
145 electrostatic and magnetic optics, the aberrations generated by electrostatic optics are often larger than those caused  
146 by their magnetic counterparts, see e.g. [36]. We therefore explored the aberrations induced by quadrupoles as they  
147 are the main focusing lenses in an electrostatic ring. An in-depth investigation into these non-linear effects,  
148 complementing commonly used design procedures, had not been realized for any of the existing or planned  
149 electrostatic storage rings.

150

151 The field components that act on a charged particle in linear beam optics approximation are dipole fields to bend  
 152 particles along a radius  $\rho$  and quadrupole fields to focus the beam with a focusing strength  $k$ . In this case, the  
 153 transverse electric field in x direction can be written as:

154

$$\begin{aligned}
 E_x &= [E_x]_{x=0} + \left(\frac{dE_x}{dx}\right)_{x=0} x \\
 &= E_{x0} \left(1 - \frac{n}{\rho} x\right)
 \end{aligned} \tag{3}$$

157

158 Here, the index  $o$  refers to an on-axis particle,  $x$  and  $\rho$  are the horizontal displacement from the design trajectory and  
 159 the local radius of curvature, respectively. From (1) one knows that  $E_{x0} = 2T/(q\rho)$  and  $n$  defines the field index.

160 On this basis, the general equations of motion in the horizontal and vertical planes can be written as [31]:

161 On this basis, the general equations of motion in the horizontal and vertical planes can be written as [31]:

162

$$\text{(Horizontal)} \quad \frac{d^2x}{ds^2} + \left[\frac{(3-n)}{\rho^2} - k\right] x = \frac{1}{\rho} \frac{\Delta T}{T} \tag{5}$$

$$\text{(Vertical)} \quad \frac{d^2y}{ds^2} + \left[\frac{(n-1)}{\rho^2} + k\right] y = 0 \tag{6}$$

165

166 where  $s$  is the position along the beam axis and  $\Delta T$  the energy spread.

167

168 Since the distribution of the field strengths  $1/\rho$  and  $k$  change along the nominal orbit, it is impossible to derive direct  
 169 analytical solutions for the trajectory equations (5) and (6). The layout therefore is started by using an abrupt-field  
 170 boundaries-model for all ion optical elements where the field begins and ends abruptly at the entrance and exit of  
 171 each electrode. In this idealization, one can represent the whole ring in matrix form by multiplying the different  
 172 transfer matrices of all ion optical elements. This approach is integrated in established simulation packages, such as  
 173 COSY Infinity [37] and MAD-X [38], and can also be easily implemented in purpose-written codes. These studies  
 174 then need to be complemented by a more detailed analysis including realistic field distributions, using for example  
 175 programs such as SIMION [39, 40], OPERA3D [41] or CPO [42]. The present design study is based on SIMION  
 176 version 8, supported by purpose-written routine and the MAD-X code.

177

178

179

### 180 3. Ion Optical Elements

181 The optical elements that make up the lattice of the of the ring design consist of dipoles for beam bending and  
182 quadrupoles for beam modulation, interconnected by field-free drift regions. In the design of an electrostatic storage  
183 ring, bending is either realized by cylinder deflectors or pair of deflecting plates. The latter are also used for beam  
184 injection and extraction. Field-free regions are used for decoupling the fields from different optical components, as  
185 well as for accommodating beam diagnostics devices and experimental setups. In the following paragraphs, an  
186 overview of the design of all elements is given.

187

#### 188 3.1. Parallel-Plate Deflector

189 Parallel-Plate Deflectors (PPDs) have been designed for beam injection and small angle deflection;  $\theta < 15^\circ$ . Here,  
190 the design is optimized for deflecting the beam by an angle of  $\theta = 7^\circ$ . This is significantly smaller than the deflecting  
191 angle in existing rings, which range between  $10^\circ$  and  $15^\circ$ . This allows us to lower the switching voltage during beam  
192 injection and hence reduces switching times and injection effects. A second advantage in lowering the deflection  
193 angle is that the effect of aberrations may be reduced [43]. As the deflectors stretch into a curved vacuum chamber it  
194 was not possible to design a shield geometry similar to all other optical elements. Even so, the support of the  
195 deflecting plates itself provides a limiting effect on the fringe field at the beam entrance side of this deflector. An  
196 illustration of such a PPD is shown in Fig. 1, and its main design parameters are summarized in Table 1.

197

198

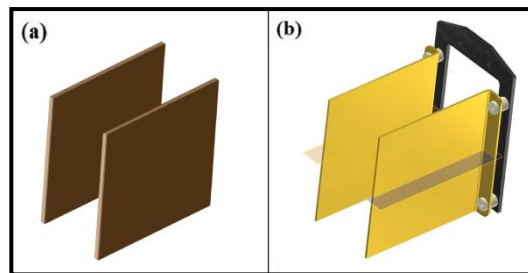
199

200

201

202

203



204 Figure 1: Design of the Parallel-Plate Deflector (PPD). (a) Design used in SIMION simulations (b) PPD with the support of the  
205 deflecting plates as designed by Inventor 3 of AutoDesk.

206

207

#### 208 3.2. Cylinder Deflector

209 Using (5) and (6) the equation of motion in a cylinder deflector, where  $n=1$ , can be written as:

210  $n=1$  describes the field in a cylindrical deflector and  $n=2$  the field in a spherical deflector.

211 (Horizontal)  $\frac{d^2x}{ds^2} + \frac{2}{\rho^2}x = \frac{1}{\rho} \frac{\Delta T}{T}$  (7)

212 (Vertical)  $\frac{d^2y}{ds^2} = 0$  (8)

213

214 It can be seen from (7) that there is a weak focusing effect, which contributes to the Betatron oscillations in the  
 215 horizontal plane, while (8) shows that the cylinder deflector acts as a field-free drift region in the vertical plane. This  
 216 is in contrast to spherical deflectors where a focusing effect is found in both transverse planes. Measurements  
 217 showed that in this case non-linear fields lead to a significant reduction in dynamic aperture and even beam losses at  
 218 higher beam intensities [44]. In this design of a 7° deflection in a PPD, a cylinder deflector with a central radius of  
 219  $\rho=250\text{ mm}$  bends the beam by an angle of  $\beta=166^\circ$ . Its main nominal parameters are also included in Table 1. An  
 220 illustration of 166° cylinder deflector set-up, including its shields, is shown in Fig. 2. This figure also shows the  
 221 vertical steerer located 10 mm upstream of the entrance shield of the cylinder deflector.

222

223

224

225

226

227

228

229

230

231

232

233

234

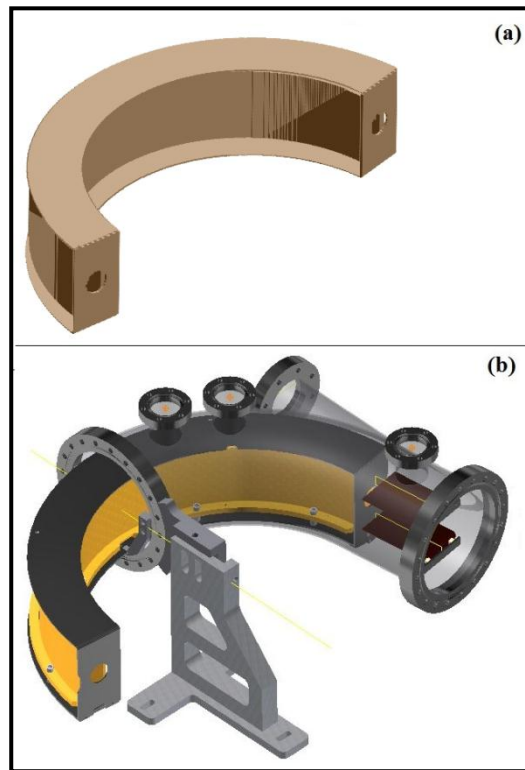
235

236

237

238

239



240 Figure 2.: Layout of the cylinder deflector set-up including longitudinal and lateral grounded shields (a) Design used in SIMION  
 241 simulations (b) Cylinder deflector set-up inserted in its vacuum chamber together with the Vertical Steerer (the pair of parallel-plates in  
 242 brown) as designed by Inventor 3.

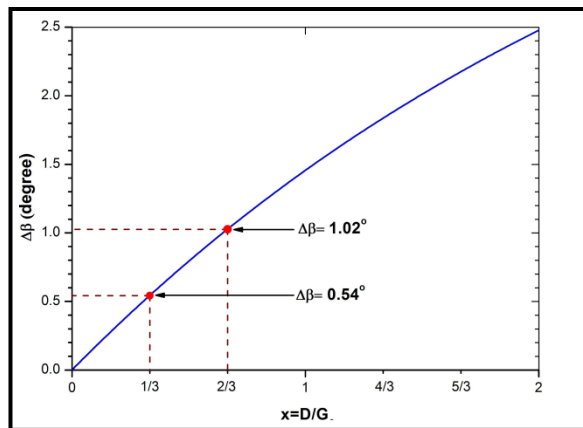
243

244 The position of the effective field boundaries have been calculated to evaluate the effects caused by fringe  
 245 fields on the beam. Among others, this allows the effective length of the deflector to be determined. The effective  
 246 deflecting angle of the cylinder deflector can then be estimated from the following parametric function [45]:  
 247

$$248 \quad \Delta\beta = \frac{G_o}{\pi\rho} \left[ \ln \left[ \frac{4}{(x^2+4)} \right] - 2x \arccos \left[ \frac{x}{\sqrt{(x^2+4)}} \right] \right] \quad (9)$$

249  
 250 Here,  $\Delta\beta$  is the extension of the bending angle due to the fringe field,  $G_o$  is half of the width of the separation gap  
 251 between the electrodes,  $\rho$  is the radius of curvature of the design orbit, i.e. the central radius of curvature in the  
 252 centre between both electrodes, and  $x=D/G_o$  is the separation distance between the electrodes and the grounded  
 253 shield, normalized to  $G_o$ .  
 254

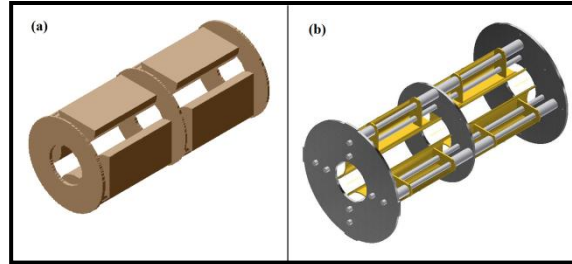
255 Function (9) is illustrated in Fig. 3. As can be seen, it yields a bending extension of  $\Delta\beta=1.02^\circ$ . In terms of  
 256 optical structure, this extension of the bending angle needs to be taken into account when determining the  
 257 geometrical length of the deflector electrodes. Final adjustment will then be realized during operation by small  
 258 changes in electrode voltages. Moreover, formula (9) allows us optimize the geometry of the entire deflector setup  
 259 and in particular the best shield configuration that minimizes or even fully compensates the fringe fields effect [43].  
 260 One can see from Fig. 3 that the bending extension reduces to  $\Delta\beta\sim 0.54^\circ$ , if  $D$  is reduced to  $5\text{ mm}$ . This then requires  
 261 a rather small geometrical adjustment that can normally be compensated by slight adjustment of the voltage on the  
 262 electrodes.  
 263



273 Figure 3: Extension of the bending angle caused by the fringe field as a function of  $x=D/G_o$ .  
 274

### 275 3.3. Quadrupole Doublets

276 Similar to magnetic quadrupoles, electrostatic quadrupoles defocus in one plane, while focusing in the other.  
277 Consequently, in the design of an electrostatic storage ring, quadrupole doublets have to be used to achieve a net  
278 focusing effect in both transverse planes. Design of the quadrupole doublets that will be used in the KACST storage  
279 ring is shown in Fig. 4., and their nominal parameters are listed in Table 1.



286  
287 Figure 4: Design of the quadrupole doublet with grounded shields. (a) As included in SIMION simulations. (b) Technical design drawing  
288 as designed by Inventor 3 of AutoDesk.

289  
290  
291 In order to decouple the fields in the doublet, the quadrupoles are designed to be set apart from each other by 33  
292 mm. In addition, the design includes a central shield inserted equidistantly between the quadrupoles. This reduces  
293 any possible coupling effects between the two quadrupoles and allow for tuning the focusing strength in the  
294 horizontal and vertical planes individually. To quantitatively determine the coupling effect between the quadrupoles  
295 in a doublet, the field distribution was calculated for the following voltage settings:

296  $(V_{QF}, V_{QD}) = (405, 360), (405, 405), (405, 0)$  and  $(0, 360)$ .  $V_{QF}$  and  $V_{QD}$  are in units of volts as applied to the  
297 focusing quadrupole (QF) and defocusing quadrupole (QD), respectively. These settings correspond to a stable  
298 working point  $(405, 360)$ , a configuration where both quadrupoles have identical, but opposite strengths, the  
299 individual action of QF, and finally the individual action of QD. Fig. 5 illustrates the simulated field distributions at  
300 a position  $x=5 \text{ mm}$  from the optical axis of the quadrupole. The illustration shows that the zero-field crossing is  
301 exactly in the middle of the central shield, when  $V_{QF}$  and  $V_{QD}$  are equal in absolute value, while it moves away from  
302 the middle of the shield by  $\sim 0.5 \text{ mm}$  at the working point. This variation is the fact of the difference between  $V_{QF}$   
303 and  $V_{QD}$  and is thus too small to be seen in the figure. A very small coupling effect between the two quadrupole  
304 fields can be observed in a region of about 60 mm around the central shield.

305

306        Quadrupoles are responsible for modulating the transverse beam shape in the ring and are the dominant factor in  
 307 causing betatron oscillations in both, the horizontal and vertical planes. For this reason, the quadrupoles are the most  
 308 important ion optical element to be considered when it comes to determining the stability of the beam storage in an  
 309 electrostatic ring. In the following the simulated quadrupole strengths are numerically scanned over a wide range to  
 310 determine the theoretical stability regions.

311

312

313

314

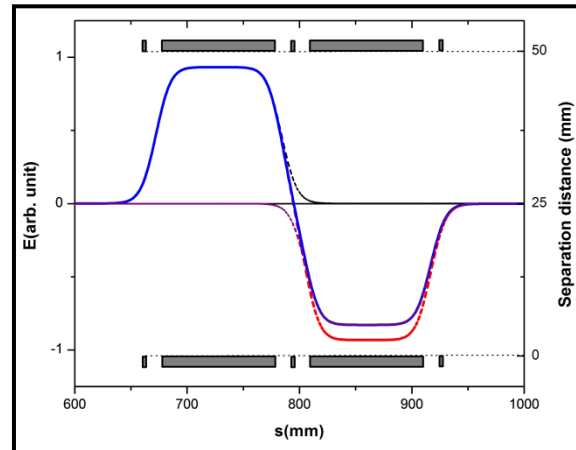
315

316

317

318

319



320

321 Figure 5: Field distributions in the quadrupole doublet at an off-axis position of  $x=5\text{mm}$  above the nominal orbit, as calculated by  
 322 SIMION for the different voltages settings ( $V_{QF}$ ,  $V_{QD}$ ) in units of Volt. The blue curve shows one of the working points with a  
 323 voltage setting of (405, 360), identical absolute voltages of (405, 405) are used for the red curve, a single focusing quadrupole  
 324 (405, 0) is used for the dashed red curve and a single defocusing quadrupole (0, 360) is illustrated by the dashed blue curve.

325

326

327        Electrostatic quadrupoles generate aberrations of octupole order [36, 46], which can potentially disturb a  
 328 traversing particle beam. For this reason, it is of high interest to calculate the aberrations induced by the ring's  
 329 quadrupoles and thus evaluate their significance with respect to beam divergence and energy spread. Several  
 330 methods for calculating the aberrations of electrostatic lenses are described in literature [47, 48], with an excellent  
 331 study on the subject by Sise, *et al* [35]. The latter carried out ray-tracing simulations using the SIMION and  
 332 LENSYS programs, and investigated the spherical and chromatic aberration coefficients of multi-element  
 333 electrostatic lens systems in great detail. A similar method has been applied in the present study. Chromatic and  
 334 spherical aberrations have been calculated for the quadrupole, using the ray-tracing simulation program SIMION  
 335 [49, 50].

336 As an example, the results shall be illustrated for the case where voltages of  $V_{QF} = 405$  V are used at a beam  
 337 energy of 30 KeV. Assuming that particles originate from a point source at position  $O$ , which is the median point  
 338 between two quadrupole doublets, the evolution of these aberrations as a function of the beam divergence angle  $\alpha$ ,  
 339 defined at origin  $O$ , is shown in Fig. 7 and follows a parabola:

$$340 \Delta r = -MC_s \alpha^3 \quad (10)$$

343 Here,  $\Delta r$  is the radius of the disk of least confusion induced by spherical aberrations,  $M$  is the linear magnification of  
 344 the lens,  $\alpha$  is the half-angle of the beam divergence and  $C_s$  is the spherical aberration coefficient, which depends on  
 345 the ion optical system. A fit on the value of the radius of the aberration disk as function of  $\alpha$  then allows us to define  
 346 how these aberrations grow with the half-angle of beam divergence and how important they are, in particular at the  
 347 maximum value of beam divergence. In the case studied here, the factor of the parabolic growth of spherical  
 348 aberrations is about 11,100 mm/radian<sup>3</sup>, yielding thus an aberration disc radius  $\Delta r = 200 \mu m$  for  $\alpha = 1.5^\circ$ , which is the  
 349 maximum half-angle of the beam divergence assumed also for all other calculations such as the MAD-X lattice  
 350 calculations.

352 Chromatic aberrations have been calculated in a similar way, again assuming a maximum beam divergence of  
 353  $\alpha = 1.5^\circ$  and their evolution as a function of relative energy spread of the beam  $\Delta T/T$  is shown in Fig. 7. The energy  
 354 spread  $\Delta T$  goes up to 20 eV, which is a typical value for the energy spread from a standard Penning ion source like  
 355 the one that will be used for initial operation of the ring. This figure shows a linear evolution of chromatic  
 356 aberrations in agreement with:

$$357 \delta r = -MC_c \alpha \frac{\Delta T}{T} \quad (11)$$

358 Here  $\delta r$  is the radius of the disk of least confusion induced by chromatic aberrations. A fit to the values of the radius  
 359 of the aberration disk as function of  $\Delta T/T$ , allows us to define how chromatic aberrations grow with a change in  
 360 kinetic energy of the particles and how significant they can be. In the case discussed here, the linear growth factor of  
 361 the chromatic aberrations is about 44.1 mm, yielding an aberration disc radius of  $\delta r = 30 \mu m$  for  $\Delta T = 20$  eV. This  
 362 does not necessary mean that spherical aberrations are dominant over chromatic ones, since the value of  $\Delta T = 20$  eV

366 only allows us to estimate the "natural" chromaticity and may be far lower than the change in energy induced by the  
 367 electrostatic bends.

368

369

370

371

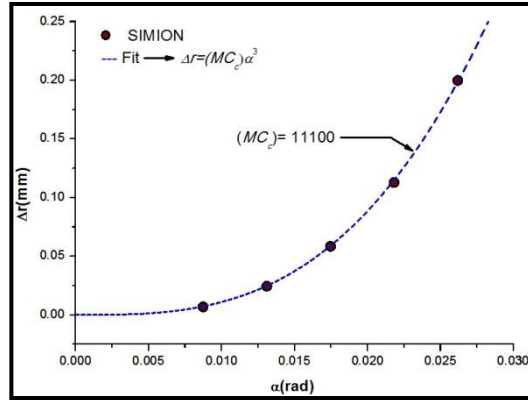
372

373

374

375

376



377 Figure 6: Evolution of spherical aberrations induced by the quadrupole. The radius of the aberration disc  $\Delta r$  is plotted as a function of the  
 378 half angle  $\alpha$  of the beam divergence at origin  $O$ . The aberrations disc is calculated in the range  $0.5^\circ < \alpha < 1.5^\circ$ , using the simulation  
 379 program SIMION.

380

381

382

383

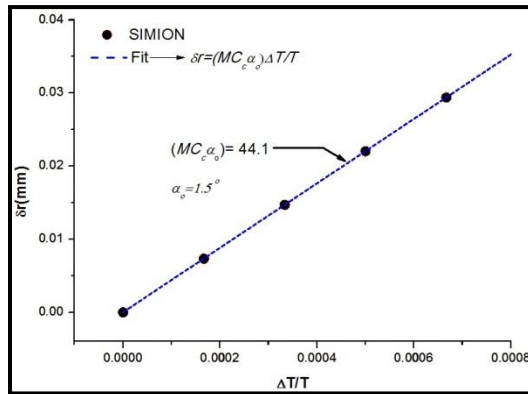
384

385

386

387

388



390 Figure 7: Evolution of chromatic aberrations, induced by the quadrupole. The radius of the aberration disc  $\delta r$  is plotted as a function of  
 391  $\Delta T/T$ , with  $\Delta T$  ranging from 0 to 20 eV. The plot is calculated using the SIMION program.

392

393

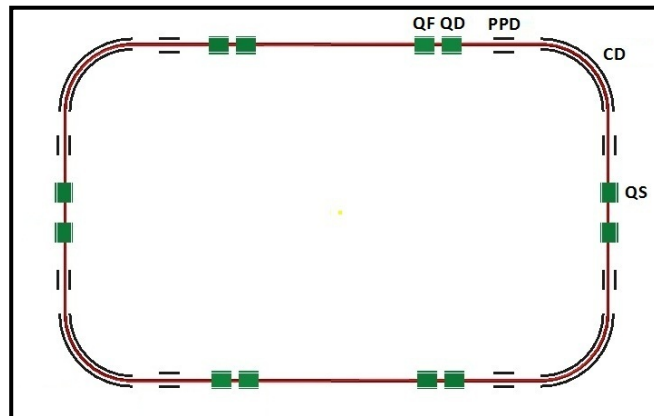
## 394 1. Storage Ring Layout

### 395 4.1 Split-bend Layout

396 The initial layout of the KACST storage ring consists of four super periods with double mirror symmetry, as  
 397 illustrated in Fig. 8. Each period constitutes one quarter of the ring and this design was chosen to allow for a future  
 398 upgrade of the ring to a double storage ring structure [31]. In this design, the bending is split into two identical

399 bending corners, consisting of a  $76^\circ$  cylinder deflector ( $76^\circ$  CD), equidistantly inserted between two  $7^\circ$  parallel-plate  
 400 deflectors ( $7^\circ$  PPDs). These form a  $90^\circ$  bending corner, connected on one side to a doublet of focusing and  
 401 defocusing quadrupoles (QF, QD) and on the other side to a quadrupole singlet (QS). A vertical steerer (VS) is  
 402 designed to be mounted on each side of the  $76^\circ$  CD for closed-orbit corrections in the vertical plane. The space  
 403 between the different optical elements is kept field-free and is designed to accommodate beam diagnostics devices  
 404 and experimental setups. From a beam dynamics point of view a lattice with only one central quadrupole singlet,  
 405 equidistantly inserted between two  $7^\circ$  PPDs in the short straight section of the ring, would also work. However, it  
 406 was decided to split this focusing action into two adjacent quadrupole singlets to be able to insert an experiment in  
 407 the middle of the short straight section where the beam can be focused down to a small diameter [43]. A  
 408 comprehensive beam dynamics study of this split-bending deflector layout goes beyond the scope of this paper and  
 409 shall be the subject of further investigations that will include the effects from the non-linearity of the fields. Here, we  
 410 limit the study to the single-bend design.

411  
 412



421  
 422  
 423  
 424

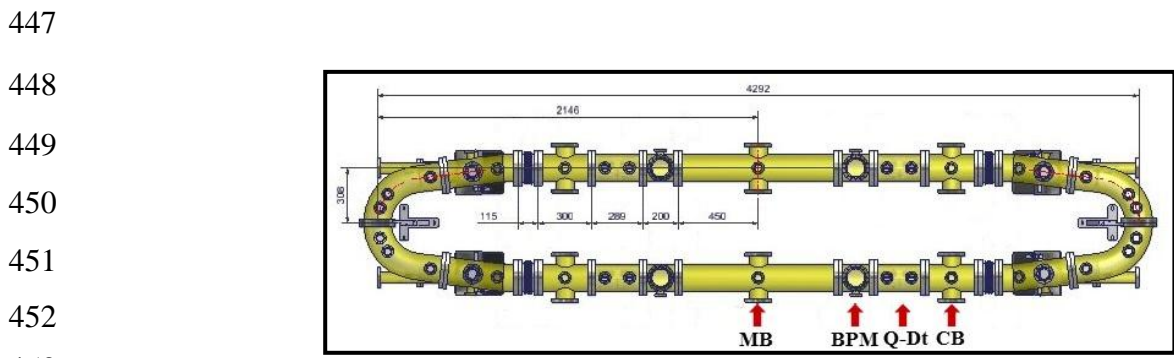
Figure 8: Lattice of the split-bend layout. QF: Focusing Quadrupole, QD: Defocusing Quadrupole, PPD: Parallel-Plate Deflector, CD: the Cylinder Deflector, (QS) Quadrupole Singlet.

#### 4.2 Single-bend Racetrack Layout

426 For practical reasons, priority is given to a quick realization of a simple and early-run adaptation of the ring,  
 427 followed by a later upgrade to the ultimate split-bend layout of the ring. In terms of design, this results in a  
 428 simplification of the lattice presented in the previous section to a racetrack layout with a single  $166^\circ$  bend and two  $7^\circ$   
 429 Parallel-Plate Deflectors ( $7^\circ$  PPDs) , see Fig. 9. This configuration avoids the need of any quadrupole singlet and

430 significantly reduces the required number of ion optical elements. Thereby, it also shrinks the size of the ring, also  
431 simplifying certain beam dynamics studies and e.g. allowing the whole storage ring to be incorporated into a single  
432 instance of the SIMION simulation [43]. This configuration comes at the expense of slightly reducing the flexibility  
433 of the facility with regard to experimental opportunities. In the following, the description will be limited to this ring  
434 layout.

435  
436 The configuration just described leads to a racetrack shaped ring with a circumference of roughly 9.2 m. Its  
437 detailed design is shown in Fig. 9. This single-bend racetrack design composes of two long straight sections that are  
438 connected by a U-turn bend that consists of a  $166^\circ$  CD, inserted in between two  $7^\circ$  PPDs. Closed-orbit corrections  
439 are realized by means of four vertical steerers (VS), designed to be located in the field-free region between the  
440 parallel-plate and cylindrical deflectors. Each straight section contains two quadrupole doublets (QF, QD), two field-  
441 free regions reserved for beam diagnostics, a central experimental section, 900 mm in length, for merged-beams  
442 experiments, and two shorter experimental sections 300mm long for crossed-beam experiments. The latter are  
443 adjacent to the  $7^\circ$  PPD thus enlarging the angular acceptance of the detector at the end of the long straight section  
444 and hence improving the collection of strongly divergent particles. The central section would even be large enough  
445 to integrate a small electron cooler similar to the one in the KEK-ring. The main design parameters of this layout are  
446 summarized in Table 1.



454 Figure 9.:  $7^\circ$ single-bend racetrack layout, as designed by Inventor 3 of AutoDesk.

455  
456 In this configuration, the beam will be injected into the ring through one of the  $7^\circ$  Parallel-Plate Deflectors  
457 (PPDs) that would be switched off during injection and switched on right after single shot filling of the ring. The rise  
458 time of the field in the small angle deflector is of the order of 10% of the revolution time of the beam in the ring and  
459 hence should not have negative effects on the beam. Transverse modulation of the beam will be realized by four  
460 quadrupoles doublets (QF, QD) and parallel-plate vertical steerers will be used for closed-orbit corrections.

461 Table 1: Design parameters of the 7° single-bend racetrack layout.

Parameters	Nominal value
Nominal beam energy [KeV·q]	30
Circumference [m]	9.2
Revolution time of protons[ $\mu$ s]	3.8
Parallel-Plate Deflector	
Nominal Deflection angle [ $^{\circ}$ ]	7
Plate area [mm $\times$ mm]	100 $\times$ 100
Electrode separation [mm]	50
Nominal voltage [kV]	$\pm 1.8$
Cylinder Deflector	
Nominal deflection angle [ $^{\circ}$ ]	166
Height [mm]	100
Central radius [mm]	250
Electrode separation [mm]	30
Electrodes-shield separation	10mm
Nominal voltage [KV]	$\pm 3.6$
Quadrupole Doublet	
Inscribed radius [mm]	25
electrode length [mm]	100
Separation gap [mm]	33
Nominal voltage [kV]	$\pm 1$

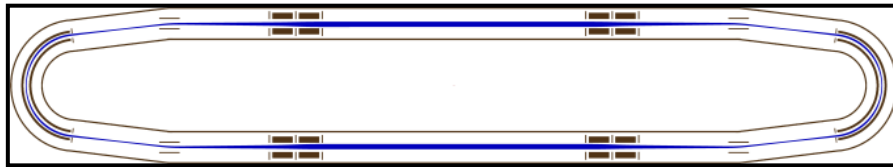
## 489 2. Beam Tracking - Stability

490 The SIMION simulation program allows charged-particles to be tracked through the real 3D field distribution,  
 491 including non-linear effects from e.g. the fringe fields. In preliminary studies [31, 51] the different components of  
 492 the lattice were individually modeled in separate geometry files and ions were then tracked through half of the ring  
 493 lattice, using SIMION's IOB operation [50]. This approach leads to some inconsistencies in overlapping regions.  
 494 Due to the limited extent of the individual geometries it also somehow idealized the field distributions and could not  
 495 take fringe fields and other non-linear effects correctly into account. Consequently, it was not possible to track ions  
 496 through the real field and 'store' them in the simulated ring, nor to study beam stability, lifetime and other important  
 497 effects in detail. Here, the geometry was built on the basis of the ring's triple mirror symmetry [52]. This enables the  
 498 size of the geometry file to be significantly reduced and the whole storage ring to be represented and incorporated in  
 499 a single instance, with one point per millimeter resolution. The only effect that cannot be correctly implemented in  
 500 this case is the action of the vertical steerers, as they require voltages of different polarity on either electrode. In  
 501 addition, SIMION's in-built geometry feature for more complex geometries have been exploited to accurately model  
 502 the cylindrical deflector including its longitudinal and lateral shields and to provide the possibility to optimize the  
 503 effective lengths of the CD. It should be pointed out that the single-bend racetrack design is small enough that it  
 504 was even possible to include all vacuum chambers in the design and to thus track ions through the most realistic

505 distribution of the fields. In this way, ions were successfully "stored" in the simulated ring for tens of thousands of  
506 turns, see Fig. 10. First simulation runs were performed to probe the ability of the ring to store low-energy beams,  
507 and a 30 KeV proton beam of diameters up to 15 mm in the centre of the long straight section was stably stored in spite  
508 of fringe fields, i.e. without any adjustment of the geometrical length of the CD's electrodes. Further simulation runs  
509 were then performed with an optimized lattice in which the cylindrical deflector setup including its shield was  
510 adjusted according to formula (9). In both cases the number of turns was very large and no difference between the  
511 two lattices in terms of beam stability was visible. However, limitations in ring acceptance and dynamic aperture  
512 were clearly observed in the case of the non-optimized lattice where fringe fields have not been adequately  
513 constrained. A more detailed analysis of these effects is the subject of further studies [53].

514

515



516

517

518 Figure 10: Cut-view of the simulated storage ring, in SIMION. In blue: a beam of 15 mm diameter is stored in the ring for thousands of  
519 turns.

520

521 In additional studies, this geometry allowed us to modify and optimize the voltage settings on all electrodes, using  
522 the SIMION in-built fast adjust scaling routine. Tuning the quadrupoles voltages over a wide range enabled  
523 numerical studies into beam stability as a function of working points to be made. Such advanced studies also allow  
524 investigations to be performed into the ring's dynamic aperture, effects from different shield geometries or the  
525 impact of positioning and field errors.

526

527 By tracking ions through the single-bend racetrack lattice and changing  $V_{QF}$  and  $V_{QD}$ , four stable regions were  
528 identified in our simulations around the working points A(405, 360), B(604, 716), C(585, 441), D (716, 760), which  
529 are in units of volts. Scanning over a range of quadrupole voltages around each working point allows us to probe and  
530 map the theoretical stable regions of the simulated storage ring. Such manual scans in a SIMION simulation,  
531 however, are very time consuming, and go beyond the scope of this paper. A detailed study will be reported  
532 separately [53].

533

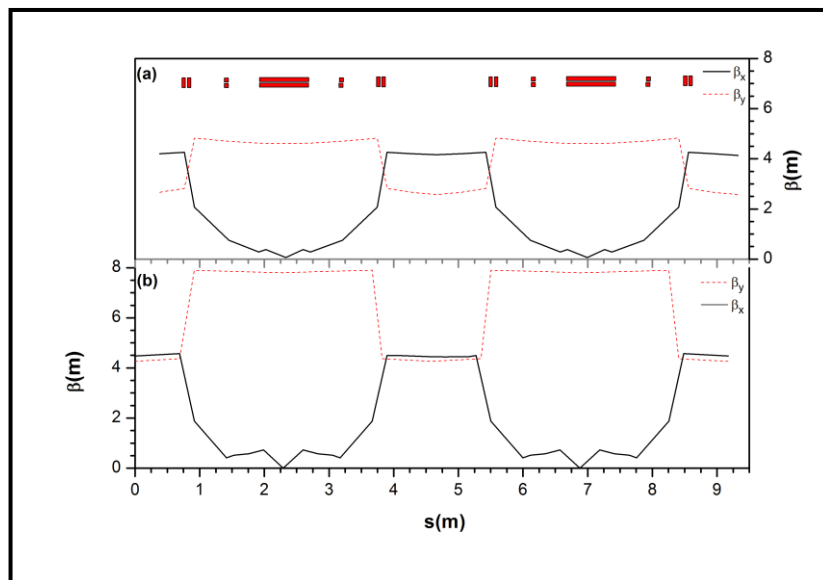
534

535 **3. Lattice Functions**

536 In its original form, MAD-X does not support electrostatic deflectors and quadrupoles. The code allows,  
537 however, the R-matrix of an arbitrary beam optical element to be implemented and lattice studies carried out similar  
538 to those normally realized for magnetic rings. Also, MAD-X has been initially written for high energy, i.e.  
539 relativistic beams, and therefore does not includes fringe fields and non-linear effects that become much more  
540 important at low beam energies. These effects have been recently studied in detail [54]. The results obtained from  
541 MAD-X, COSY Infinity and a custom-written tracking routine relying on the field maps from the OPERA3D code  
542 were benchmarked against each other, to show the limitations of each method. Likewise, the here-presented  
543 simulation makes use of the custom-written tracking routine in order to determine the working points and stability  
544 regions in the single-bend racetrack design and to compare them to the results obtained from SIMION.

545  
546 Preliminary lattice calculations have been done for the basic conceptual design [32-33]. However, the practices  
547 adopted for fringe fields limitation such as e.g. the addition of shields and others geometrical constraints and  
548 experimental requirements, imposed some changes to the optics configuration in such a conceptual design.  
549 Consequently, the lattice calculations must be revised. Here, we refined and reproduced the lattice function, using  
550 the MAD-X code for the ultimate single-bend racetrack design. Although only few quadrupoles are used in the  
551 single-bend racetrack design, the simulated ring can be set to many different operating modes, including elliptical  
552 and round beams, as illustrated in Fig. 11.

553  
554  
555  
556  
557  
558  
559  
560  
561  
562  
563  
564  
565  
566



567 Figure 11: Two different operating modes of the simulated single-bend racetrack ring as calculated using MAD-X code. Top (a): Round  
568 beam in the centre of the straight section, optimized for merged/crossed beam experiments. Bottom (b): Elliptical beam in the centre of  
569 the straight section which keeps beam dimensions minimum all around the storage ring.  
570

571 To numerically compute and delimit the theoretical stability regions of the single-bend racetrack design, a  
572 custom-written tracking routine relying on the field maps from OPERA3D [54] has been used. This routine models  
573 the ion trajectories through realistic field distributions and thus allows the stability of the beam to be probed. Fig. 12  
574 shows the theoretical stability regions as a function of Focusing (F) and Defocusing (D) quadrupole-strength,  $k_F$  and  
575  $k_D$ . The results from the tracking routine agree with those carried out using the SIMION program, which track ions  
576 in the most realistic fields. In fact, one can see that each of the afore-mentioned working points expressed in term of  
577 quadrupole strengths ( $k_F$ ,  $k_D$ ) as A(2.16, 1.92), B(1.71, 1.28), C(3.30, 1.72), D (3.65, 2.32), in units of  $m^2$ , fits into a  
578 corresponding stability region. Analysis of detailed effects clearly showed that the results from the tracking studies  
579 provided much more detailed results than those that could be obtained by using MAD-X. In some cases, limitations  
580 of using an R-Matrix based approach when studying beam stability and dynamic aperture were clearly observed and  
581 priority should be given to studies based on the real three-dimensional field distribution.  
582

582

583

584

585

586

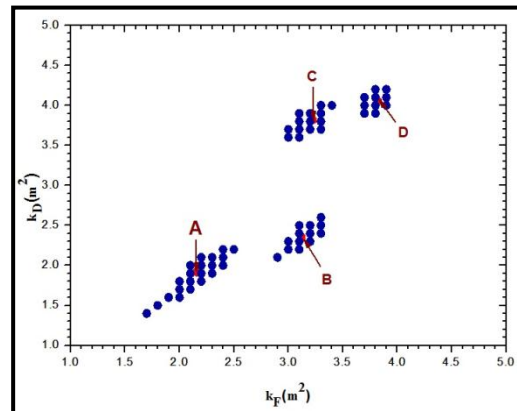
587

588

589

590

591



592 Figure 12: The four working points A-D and corresponding stability regions, as calculated using the custom-written tracking routine for  
593 single-bend racetrack design. The plot is represented in a ( $k_F$ ,  $k_D$ ) diagram where  $k_F/k_D$  are the absolute value of the quadrupole strength.  
594

594

595

596

597

598

599

600 Table 2.: Lattice parameters of the 7° single-bend layout for an elliptic beam.

601

Parameters	Value
Emittance [ $\pi$ mm mrad]	15
Acceptance [ $\pi$ mm mrad]	25
Lattice Functions	
$\beta_{x, \text{initial}}$ [m]	4.2
$\beta_{y, \text{initial}}$ [m]	2.6
$\beta_{x, \text{min}}$ [m]	0.1
$\beta_{y, \text{max}}$ [m]	4.8
Nominal voltage [kV]	$\pm 3.6$
Betatron Tunes	
$Q_x$	.74
$Q_y$	.2
Chromaticity	
$\xi_x$	-3.1
$\xi_y$	-2.2
Quadrupole Strengths	
$k_{QF}$ [ $\text{m}^{-2}$ ]	2.2
$k_{QD}$ [ $\text{m}^{-2}$ ]	-1.8

602

603

604

605

606

#### 4. Conclusion

607

608

609

610

611

612

613

614

615

616

617

The design of a 7°-electrostatic storage ring that can store ions with energies of up to 30keV.q and that is being in development at KACST, was presented in this paper. Although this experimental facility shall consist of a double ring configuration in its final phase, allowing for a very broad and interdisciplinary research program, it was decided to start with a simpler, but quicker to realize 'start version'. This small storage ring will already offer many exciting research opportunities for local researchers as well as for the international research community. In this paper details on the 7°-design of the storage ring were presented with an emphasis on an accurate simulation of the effects from non-linear fields and the results from simulation studies with SIMION. The present design study has complemented and finalized the design of the 7° single-bend racetrack-shaped electrostatic storage ring at KACST.

#### Acknowledgments

618

619

620

621

622

623

M. O. A. El Ghazaly who initiated and leads this project for building the electrostatic storage ring at KACST (Pro-ESR), gratefully thanks S P Møller for comments related to SIMION implementations and advice in designing the electrostatic storage ring. Valuable discussions with P. Defrance are also gratefully acknowledged. Thanks go to Henrik Juul at the University of Aarhus for help in the mechanical design, and to the NCMP technicians at KACST for their efforts related to this work. This project is funded by KACST under the grant no. 162-28/MOA\_El Ghazaly. M.O.A El Ghazaly (project PI) gratefully thanks KACST for this grant.

624 **References**

- 625 1. S.P. Møller,  
626 Nucl. Instr. and Meth. A 394 (1997) 281.
- 627 2. L H Andersen, O Heber and D Zajfman  
628 J. Phys. B: At. Mol. Opt. Phys. **37** (2004) R57–R88.
- 629 3. T. Tanabe, K. Chiba, K. Noda, I. Watanabe,  
630 Nucl. Instr. and Meth. A **482** (2002) 595c.
- 631 4. U. V. Pedersen, M. Hyde, S. P. Møller, and T. Andersen,  
632 Phys. Rev. A **64**, 012503 (2001).
- 633 5. K. Hansen, J.U. Andersen, P. Hvelplund, S.P. Møller, U.V. Pedersen, V.V. Petrunin,  
634 Phys. Rev. Lett. 87 (2001) 123401
- 635 6. S. B. Nielsen, A. Lapierre, J. U. Andersen, U. V. Pedersen, S. Tomita and L. H. Andersen,  
636 Phys. Rev. Lett., 2001, 87, 2281021
- 637 7. J. U. Andersen, P. Hvelplund, S. Brøndsted Nielsen, S. Tomita, H. Wahlgreen, S. P. Møller, U. V. Pedersen, J. S. Forster, and  
638 T. J. D. Jørgensen  
639 Rev. Sci. Instrum. **73**, 1284 (2002).
- 640 8. L. H. Andersen, I. B. Nielsen, M. B. Kristensen, M. O. A. El Ghazaly, S. Haacke, M. Brønsted Nielsen, and M. Åxman  
641 Petersen.  
642 J Am Chem Soc. (2005) 127(35):12347-12350
- 643 9. I.B. Nielsen, S. Boyé.–Peronne, M.O.A. El Ghazaly, M.B. Kristensen, S. Brøndsted Nielsen, and L.H. Andersen:  
644 Biophys. J., **89** 2597-2604 (2005)
- 645 10. H. Bluhme, M. J. Jensen, S. B. Nielsen, U. V. Pedersen, K. Seiersen, A. Svendsen, and L. H. Andersen,  
646 Phys. Rev. A **70**, 020701 (2004)
- 647 11. Tanabe T, Noda K and Syresin E,  
648 Nucl. Instrum. Meth. Phys. Res. Sect. A **532** (2004) 105.
- 649 12. T. Tanabe, K. Noda, M. Saito, S. Lee, Y. Ito, H. Takagi,  
650 Phys. Rev. Lett. 90 (2003) 193201.
- 651 13. T. Tanabe, K. Noda, M. Saito, E.B. Starikov, M. Tateno,  
652 Phys. Rev. Lett. 93 (2004) 043201.
- 653 14. M. O. A. El Ghazaly, A. Svendsen, H. Bluhme, A. B. Nielsen, S. Brøndsted Nielsen, and L. H. Andersen Phys. Rev. Lett. **93**,  
654 203201 (2004)
- 655 15. A. Svendsen, H. Bluhme, M. O. A. El Ghazaly, K. Seiersen, S. B. Nielsen, and L. H. Andersen,  
656 Phys. Rev. Lett. 94, 223401 (2005)
- 657 16. Steen Brøndsted Nielsen, Lars H. Andersen,

- 658 Biophysical Chemistry 124 (2006) 229–237
- 659 17. S Brøndsted Nielsen, J U Andersen, P Hvelplund, B Liu and S Tomita,  
660 J. Phys. B: At. Mol. Opt. Phys. 37 (2004) R25–R56
- 661 18. T Tanabe,  
662 J. Phys.: Conf. Ser. **58** (2007) 17–24
- 663 19. S. Jinno, T. Takao, Y. Omata, A. Satou, H. Tanuma, T. Azuma, H. Shiromaru, K. Okuno, N. Kobayashi, I. Watanabe,  
664 Nucl. Instr. and Meth. A **532** (2004) 477c
- 665 20. S. Jinno, T. Takao, K. Hanada, M. Goto, K. Okuno, H. Tanuma, T. Azuma, H. Shiromaru  
666 Nucl. Instr. and Meth. A **572** (2007) 568–579
- 667 21. A. E. K. Sundén, M. Goto, J. Matsumoto, H. Shiromaru, H. Tanuma, T. Azuma, J. U. Andersen, S. E. Canton, and K. Hansen  
668 Phys. Rev. Lett. 2009, 103, 143001
- 669 22. K.E. Stiebing, V. Alexandrov, R. D'orner, S. Enz, N. Yu. Kazarinov, T. Kruppi, A. Schempp, H. Schmidt Bocking, M. Volp,  
670 P. Ziel, M. Dworak, W. Dilfer  
671 Nucl. Instr. and Meth Phys. Res. A **614** (2010) 10–16
- 672 23. K.-G. Rensfelt et al.,  
673 "DESIREE - a Double Electrostatic Storage Ring",  
674 Proc. Europ. Part. Acc. Conf., Lucerne, Switzerland (2004)
- 675 24. R. D. Thomas, H. T. Schmidt, G. Andler, M. Björkhage, M. Blom, L. Brännholm, E. Bäckström, H. Danared, S. Das, N.  
676 Haag, P. Halldén, F. Hellberg, A. I. S. Holm, H. A. B. Johansson, A. Källberg, G. Källersjö, M. Larsson, S. Leontein, L.  
677 Liljeby, P. Löfgren, B. Malm, S. Mannervik, M. Masuda, D. Misra, A. Orbán, A. Paál, P. Reinhard, K.-G. Rensfelt, S. Rosén,  
678 K. Schmidt, F. Seitz, A. Simonsson, J. Weimer, H. Zettergren, and H. Cederquist  
679 Rev. Sci. Instrum., **82**, 065112, (2011).
- 680 25. D. Zajfman, A. Wolf, D. Schwalm, D. A. Orlov, M. Grieser, R. von Hahn, C. P. Welsch, J. R. C. Lopez-Urrutia, C. D.  
681 Schröter, X. Urbain, and J. Ullrich,  
682 J. Phys.: Conf. Ser. **4**, 296 (2005).
- 683 26. R. von Hahn, K. Blaum, J. R. C. López-Urrutia, M. Froese, M. Grieser, M. Lange, F. Laux, S. Menk, J. Varju, D. A. Orlov, R.  
684 Repnow, C. Schröter, D. Schwalm, T. Sieber, J. Ullrich, A. Wolf, M. Rappaport, D. Zajfman, X. Urbain, and H. Quack,  
685 *Proceedings of the EPAC 2008*, Genoa, Switzerland (EPS-AG, 2008), p. 394.
- 686 27. J. Bernard, G. Montagne, R. Brédy, B. Terpend-Ordacièrè, A. Bourgey, M. Kerleroux, L. Chen, H. T. Schmidt, H.  
687 Cederquist, and S. Martin  
688 Rev. Sci. Instrum. **7**, 075109, 2008.
- 689 28. Y. Nakano, Y. Enomoto, W. Morimoto, and T. Azuma, Books of abstracts, the 4<sup>th</sup> International Workshop on Electrostatic  
690 Storage Devices-ESD11, ORNL, Tennessee, June 8-11 (2011).  
691 [www-cfadc.phy.ornl.gov/ESD\\_2011/abstracts/contributed/Nakano.pdf](http://www-cfadc.phy.ornl.gov/ESD_2011/abstracts/contributed/Nakano.pdf)

- 692 29. C.P. Welsch, M. Grieser, J. Ullrich, A. Wolf  
693 Nucl. Instr. and Meth. A **546** (2005) 405c
- 694 30. Ara Chutjian, *private communication*, and Chutjian *et al.*, "*Proposal for a new electrostatic storage ring at Jet Propulsion*  
695 *Laboratory*" online.
- 696 31. M.O.A. El Ghazaly  
697 CDR- Conceptual Design Report: "*A new Electrostatic Storage ring at KACST*"  
698 R<sub>0</sub>/162-28, NCMP, KACST, Riyadh (2007); and also M.O.A. El Ghazaly, A proposal for the development of "*A new*  
699 *Electrostatic Storage ring at KACST*", Grant No. 162-28/MOA\_El Ghazaly, NCMP, KACST, Riyadh (2007).
- 700 32. M. O. A. El Ghazaly, A. A. Alzeanidi, M. Al-Malki, A. Papash, P. Schmid, and C. P. Welsch.  
701 Applied Mathematics and Information Sciences, **3** (3) 301-307 (2009).
- 702 33. M.O.A. El Ghazaly, M. Al-Malki, A.I. Papash, and C. P. Welsch,  
703 Proc. Part. Acc. Conf., Vancouver, Canada (2009).
- 704 34. M.O.A. El Ghazaly.  
705 Books of abstracts, the 4<sup>th</sup> International Workshop on Electrostatic Storage Devices-ESD11,  
706 ORNL, Tennessee, June 8-11 (2011).  
707 [www.cfadc.phy.ornl.gov/ESD\\_2011/abstracts/invited/](http://www.cfadc.phy.ornl.gov/ESD_2011/abstracts/invited/)  
708 ElGhazaly.pdf
- 709 35. Omer Sise, Melike Ulu, and Mevlut Dogan  
710 Nucl. Instr. and Meth. A **573** (2007) 329–339
- 711 36. H. Danared, L. Liljeby, G. Andler, L. Bagge, M. Blom, A. Källberg, S. Leontein, P. Löfgren, A. Paál, K.-G. Rensfelt, A.  
712 Simonsson, H. T. Schmidt, H. Cederquist, M. Larsson, S. Rosén, and K. Schmidt.,  
713 AIP Conf. Proc. 821, pp. 465-472
- 714 37. K. Makino, M. Berz, "COSY INFINITY Version 9",  
715 Nucl. Instr. Meth. A **558** (2005) 346-350.
- 716 38. <http://mad.web.cern.ch/mad/>
- 717 39. SIMION 3D v8.0, Scientific Instrument Services Inc. <http://www.simion.com>
- 718 40. David A. Dahl,  
719 Int. J. Mass Spect. 200 (2000) 3–25.
- 720 41. OPERA-3d Reference Manual, Vector Fields Ltd., England.
- 721 42. CPO programs,  
722 [www.electronoptics.com](http://www.electronoptics.com)
- 723 43. M.O.A. El Ghazaly  
724 TDR-Technical Design Report,  
725 NCMP, KACST, Riyadh (2011).

- 726 44. S.P. Møller, P. Bowe, J.S. Nielsen, and U.V. Pedersen  
727 Proc. Europ. Part. Acc. Conf., Vienna, Austria (2000).
- 728 45. Function generated using calculations from H. Wollnik "*Optics of Charged Particles*", Academic, Orlando (1987). Details on  
729 the calculations can be found in [43].
- 730 46. L.A. Baranova e F.H. Read,  
731 OPTIK, 112(3), 2001, pp. 131-138.
- 732 47. K. Saito, T. Okubo, K. Takamoto, Y. Uno, M. Kondo  
733 J. Vac. Sci. Technol. A 4 (1986) 1913
- 734 48. C.E. Kuyatt, D. DiChio, S.V. Natali,  
735 J. Vac. Sci. Technol. A 10 (1973) 1124.
- 736 49. D. A. Dahl, J. E. Delmore, and A. D. Appelhans,  
737 Rev. Sci. Instrum. 61, 607 (1990).
- 738 50. D. J. Manura, D. A. Dahl, SIMION® 8.0 User Manual.2003-2008. Scientific Instrument Services Inc., Idaho National  
739 laboratory (2008).
- 740 51. A.A. Almuqhim, et al.  
741 AIP Conf. Proc. **1370**, 278 (2011).
- 742 52. S.P. Møller, *private communication*.
- 743 53. M.O.A El Ghazaly, *in preparation*
- 744 54. D. Newton, et al.,  
745 Proc. IPAC, San Sebastian, Spain (2011).